UDC 004.852
doi:10.31799/1684-8853-2025-4-2-12
EDN: ZRIITM

Научные статьи
Articles

3D medical image segmentation with persistent homology-based constraints

R. I. Dumaev[a], *Post-Graduate Student, orcid.org/0009-0002-3674-4952*
S. A. Molodyakov[a], *Dr. Sc., Tech., Professor, orcid.org/0000-0003-2191-9449, samolodyakov@mail.ru*
L. V. Utkin[a], *Dr. Sc., Tech., Professor, orcid.org/0000-0002-5637-1420*
[a]*Peter the Great St. Petersburg Polytechnic University, 29, Politekhnicheskaia St., 195251, Saint-Petersburg, Russian Federation*

Introduction: *Medical image segmentation is a widely researched field where neural networks serve as a basis for many medical data analysis and visualization processes. Traditional approaches to training segmentation models often rely on voxel-wise loss functions, which are insufficient for many segmentation tasks, and do not consider the topological correctness of the segmentation. Consequently, masks learned by such models may be spatially inconsistent, resulting in unrealistic features such as spurious connected components or holes.* ***Purpose:*** *To develop a method for training models to improve the quality of medical 3D image segmentation by leveraging persistent homology and comparing persistence diagrams during training.* ***Results:*** *We propose a method for training 3D image segmentation models, including persistent homology-based constraints and a loss function that is used to regularize the shape and edge reconstruction process of the mask. We present a filtration function based on the distance to the centroid of a binary mask to refine the shape and edge of the predicted mask. The analysis of the results obtained during the experiments on lung computed tomography data for segmentation and target structure extraction tasks has shown the effectiveness of our approach. The proposed approach not only improves the accuracy at the voxel level, but also preserves essential morphological properties, which is extremely important for subsequent tasks, such as nodule volume estimation and clinical decision making.* ***Practical relevance:*** *The use of the presented approach makes it possible to improve the quality of lung nodule segmentation using 3D CT images.*

Keywords *— medical image segmentation, shape prediction, topological data analysis, persistent homology, lung nodule segmentation.*

For citation: Dumaev R. I., Molodyakov S. A., Utkin L. V. 3D medical image segmentation with persistent homology-based constraints. *Informatsionno-upravliaiushchie sistemy* [Information and Control Systems], 2025, no. 4, pp. 2–12. doi:10.31799/1684-8853-2025-4-2-12, EDN: ZRIITM

Introduction

In the analysis and visualization of clinical data workflows, accurate segmentation of medical images is a crucial step. For example, lung nodule segmentation plays a vital role in computer-aided diagnosis (CAD) systems for lung cancer, as it provides essential information such as nodule sizes, shapes, and other critical medical characteristics [1]. By allowing for accurate volume estimation, reliable segmentation is essential for effective nodule management, particularly when calculating volume doubling time [2, 3]. The large volume of data generated by CT imaging, which can produce hundreds of images of the lungs per second, poses a significant challenge to radiologists, who must individually examine thousands of slices in each scan for diagnostic purposes. This process is not only time-consuming and labor-intensive but also susceptible to errors [4]. Furthermore, manual segmentation is prone to observer variability, highlighting the need for an efficient and accurate automated lung nodule segmentation method to enhance the early detection rate of lung cancer.

The works [5, 6] show that there has been significant progress in the segmentation of 2D and 3D medical images. This was influenced by the advent of deep learning models and convolutional neural networks, an successful example of which is the U-Net architecture [7], which generalizes features at different levels (from local at the voxel level to global at the anatomical level) and is successfully applied in various domains. At the same time, it can be noted that less attention is paid to the process of model optimization [8] and most works use loss functions common in segmentation problems: cross-entropy, Jaccard index and Dice coefficient (which consider voxels independently and are insensitive to errors such as false connected components or holes). As a result, such loss functions are insufficient for many segmentation problems and do not take into account the topological correctness of the segmentation, which can be learned during the optimization process.

In clinical practice, the characteristics of pulmonary nodules, such as their sizes, shapes, and specific features like calcification, lung lobe, and ground-glass shadows, exhibit significant variability across different levels. In addition, the morphologic features seen on CT images often resemble those of vascular tissues, which may make accurate

segmentation of pulmonary nodules difficult and lead to spatial inconsistencies.

If spatial features are not taken into account when optimizing a convolutional neural networks, it can result in segmentations that lack spatial coherence, including spurious connected components or holes. Such errors can appear nonsensical, but they are often confined to object boundaries and may not significantly impact the assessment of specific clinical features. Nevertheless, for many downstream applications, such as nodule volume estimation [2, 3], it is essential to accurately capture these spatial features in order to ensure reliable results.

Capturing spatial consistency and boundary consistency in segmentation masks requires abstract and adaptable information that can accommodate the diverse range of cases encountered in clinical settings, rather than relying on specific examples from training data. Spatial prior consistency offers a global measure of segmentation consistency. Such measure can be applied to normal and complex pathological regions of an image, unlike conventional losses that treat voxels independently. However, while quantifying conventional loss functions is straightforward, estimating spatial prior consistency presents significant complexity and non-trivial challenges. Furthermore, explicitly integrating this measure into convolutional neural networks is hampered by the opacity of such models. We present a topological descriptor module and topological constraints to address the limitations and challenges described above.

The contributions can be summarized as follows:

— Recently, there have been some papers that use topological data analysis (TDA) together with machine learning [9]. Using TDA, it is possible to analyze the shape of objects in different dimensions and use it as an additional source of features. We propose a loss function that uses these features to help the model learn the shape and boundaries of a mask in a segmentation task.

— We propose a centroid loss that encourages the alignment of centroids between the predicted mask and the ground truth to improve optimization process.

— To capture boundary information of shape we introduce filtration based on distance to the centroid of binary mask.

Related works

Medical images segmentation

Accurate segmentation of lung nodules is a crucial component of CAD systems, as it enables the precise delineation of a target nodule's boundary. The primary objective of lung nodule segmentation is to provide detailed information about the nodule, including its diameter, size, and semantic characteristics important for diagnosis [10]. In [11], authors highlight the importance of these details for malignancy assessment of the nodule and treatment planning. The segmentation method allows for the extraction of precise boundaries of the nodule and overall size [12]. The main challenge of this task is that lung nodules have various shapes, sizes, and delicate features. Recently, deep learning has become the most popular method in this area. In [13], the authors propose a novel model called the Dual-branch Residual Network (DB-ResNet), which enhances segmentation accuracy by integrating multi-view and multi-scale feature extraction techniques. This model can handle the complexities associated with different types of lung nodules: the proposed method involves the use of features capture from three different slices (upper, middle, lower) and central intensity pooling layer, which focuses on extracting intensity features from the center voxel of the nodule.

Zhou et al. [14] proposed a cascaded multistage framework and split the process into several stages. In the localization stage 2D-based model performs initial rough localization of nodules on axial CT slices. In aggregation and segmentation stages, the candidate nodule selection algorithm refines the location of nodules and reduce redundancy among candidates and segment final masks.

Yang et al. [15] considered the problem of capturing the variability of clinical practice where different radiologists may provide different segmentations for the same nodule and designed an uncertainty-aware attention mechanism that leverages the consensus and disagreements among multiple annotations to improve segmentation performance. Their model aims to provide a more nuanced understanding of areas with varying levels of confidence.

The results of such models can be used to perform subsequent evaluation of the characteristics of the nodule [16]. Observations from previous studies suggest that current methods tend to focus primarily on improving segmentation accuracy without taking into account the spatial and boundary consistency of the predicted segmentation mask.

Segmentation with topological data analysis

Various approaches leveraging TDA have been developed to ensure the topological accuracy of objects in images [17, 18]. In [19], the authors proposed method measures the difference between high-level structural information which include concepts such as connectivity or holes captured by pretrained network for delineating curvilinear structures such as cell membranes. TDA has also been successfully applied for tumor segmentation [20] and cortical plate segmentation [21] in 3D MRI scan, cancer prediction on whole slide histology images [22], for ultrasound

imaging analysis [23] and object segmentation in microscopy images [24]. The first type of application involves designing segmentation methods that constrain their topology. For instance, researchers in [25] introduced a topological loss function, calculated using TDA, to supplement the standard loss function used in training segmentation models. By incorporating prior topological knowledge, the segmentation process is restricted to produce results that closely resemble a predefined shape. This concept has been successfully applied to segmenting the myocardium, which is known to have a ring-like shape, and to segmenting the placenta, which is recognized as a single connected component without holes.

An alternative approach, presented in [21, 26], involves training a neural network to minimize the difference between the persistence diagrams of the images and their corresponding ground truth segmentations. Rather than relying on explicit prior knowledge to constrain the persistence diagram, the authors introduce a topology-preserving loss function. It encourages the segmentation output to preserve the same topological characteristics as the ground truth, specifically by aligning the Betti numbers (which represent the number of connected components and holes) between the predicted and actual segmentation masks.

As an another application of TDA, it can be utilized to characterize the topological structure of image components. For example, in [27, 28], the authors use persistent homology to identify image patches that contain tumors, based on the presence of an increased number of holes and connected components. This approach is grounded in the fact that infected tissues often exhibit irregular nuclei shapes and sizes, which can be distinguished from healthy tissues using TDA. Finally, it is worth noting that TDA is a rapidly evolving field with ongoing research and development of new methods.

Method for training 3D segmentation models

In Figure 1 we provide a flowchart of our proposed pipeline, which include the integration of TDA, particularly persistent homology, with a new filtration function based on distance to the centroid to refine shape and boundary topology. Given a predicted mask and 3D ground truth, we calculate topological features using topological descriptor with cubical persistent homology. We compare the resulting persistence diagrams using topological constraints and combine it with centroid loss and Dice loss.

The output of the trainable model and the ground truth segmentations are sequentially processed through a topological descriptor to efficiently capture the topology information of target instances. Then we compare the resulting persistence diagrams using topological constraints and combine it with centroid loss L_C and Dice loss L_{Dice}. It encourages the segmentation output of the trainable model to preserve the same topological characteristics as the ground truth.

Topology assessment

Previous studies [29, 30] have shown that cubic complexes are effective for representing and exploring volumetric data. Topological features of different dimensions for cubical complex include

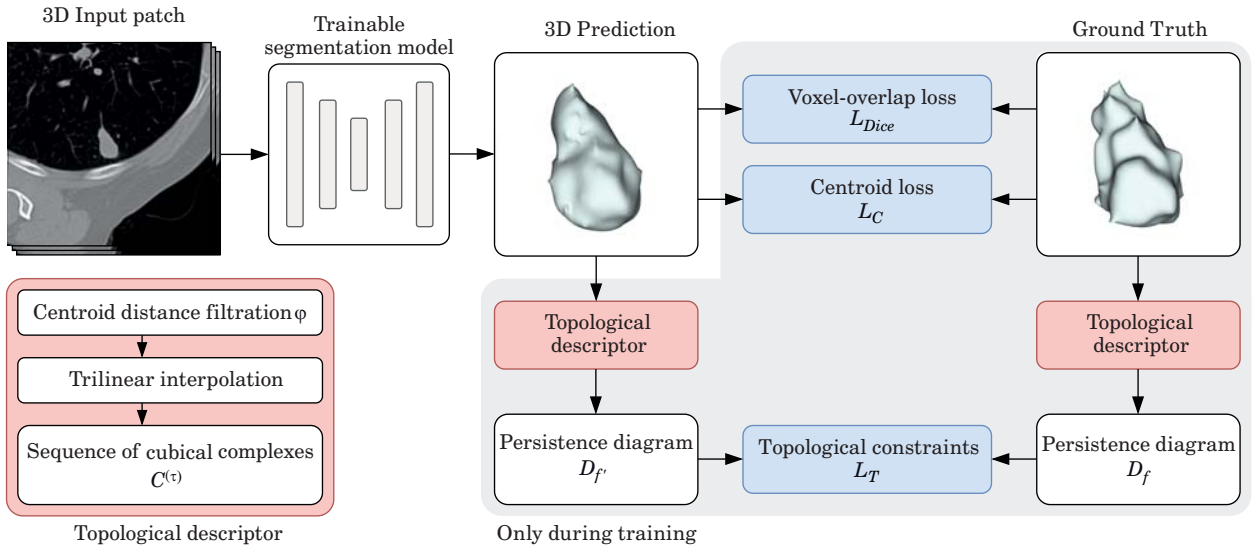

■ ***Fig. 1.*** Overview of the proposed method

connected components, cycles, and voids. We represent a volume V as a cubical complex C. A volume V can be described by a m-dimensional tensor with a shape of $n_1 \times n_2 \times ... \times n_m$. Cubical complex represents an each voxel of a volume V as vertices and their spatial relationships (points, lines, squares and cubes).

The Betti number, represented as β_k, measures the number of k-dimensional topological features, such as connected components, loops, or voids, in a cubical complex V. Betti numbers only provide a count of features and do not account for their scale or how long they persist across different resolutions. Therefore, they are limited in applications requiring multi-scale analysis, although there are works that use them in image segmentation tasks as a topological prior [31, 32]. To address this limitation we utilize persistent diagrams to enable the calculation of topological features (capturing both their presence and their persistence over varying levels of detail) across multiple scales.

To analyze the structure of the volume, we apply a threshold $\tau \in \mathrm{R}$ which filters the voxels based on their likelihood values. We get likelihood values using likelihood function $f : V \to \mathrm{R}$, learned by our model, evaluates each voxel $x \in V$, and assigns it a probability value indicating how likely it is to belong to a nodule. Specifically, a cubical complex $C^{(\tau)}$ is formed by including all voxels x that satisfy $f(x) \geq \tau$. The topology of the resulting cubical complex changes only at a finite number of thresholds $\tau \geq \ldots \geq \tau_m$ (due to the volume is finite). Thus, by applying these thresholds, we obtain super-level set filtration — a sequence of nested cubic complexes: $\varnothing \subseteq C^{(\tau_1)} \subseteq C^{(\tau_2)} \subseteq \ldots \subseteq C^{(\tau_m)} = V$ which captures the changes of the volume's topological features. In this way we can track pairs of thresholds at which k-dimensional features appear and disappear. We then define the persistence diagram $D_f^{(k)}$ as the set of pairs of such thresholds: (τ_i, τ_j), where $\tau_i \geq \tau_j$ — creation and destruction of k-dimensional features with $0 \geq k \geq m$. By monitoring these features throughout the entire filtration, persistent homology offers a detailed and comprehensive characterization of the nodule's topological structure.

In contrast to Betti numbers, which require a fixed threshold τ for the likelihood function and yield a single set of topological descriptors, persistence diagrams offer a more comprehensive representation of the data by encoding all possible thresholds simultaneously. This allows for the capture of additional geometrical details that would be lost with a single threshold choice. The persistence of a topological feature defined as $pers(\tau_i, \tau_j) = |\tau_i - \tau_j|$ for a given tuple (τ_i, τ_j) in the persistence diagram, provides a measure of the feature's scale or stability. Larger persistence values typically indicate more robust features that persist over a wider range of thresholds.

It is important to note that although the filtration can be computationally expensive, practical implementations have shown that persistent homology for cubical complexes can be computed efficiently, as highlighted in previous work [29].

We showcase an example of a filtration process from a centroid distance function in Fig. 2. Given a centroid distance function of the binary mask, as the threshold increases, various features appear and disappear. Each point on the persistence diagram represents a feature and has a creation and destruction value — interval in which it appears and disappears. Note that this is for illustrative purposes only, and in reality the resulted persistence diagram may look different, since cubical complex for this example is built from only one slice of the 3D nodule patch.

Topological descriptor

As previously noted, pixel-wise loss is insensitive to capturing spatial consistency and boundary consistency in segmentation masks. To explicitly incorporate such priors into parameter optimization and quantitatively represent them, we present a topological descriptor module.

At the input, the module receives a binary mask V and transforms it using the filter function φ. Then, for computational efficiency, we downsample each sample to reduce the dimensionality using bilinear and trilinear interpolation for 2D and 3D respectively. We provide an additional information about the impact of interpolation step in Experiments section. Based on the interpolated result, we calculate a cubic complex C. This module is used to obtain topological features, which are then compared with topological constraints.

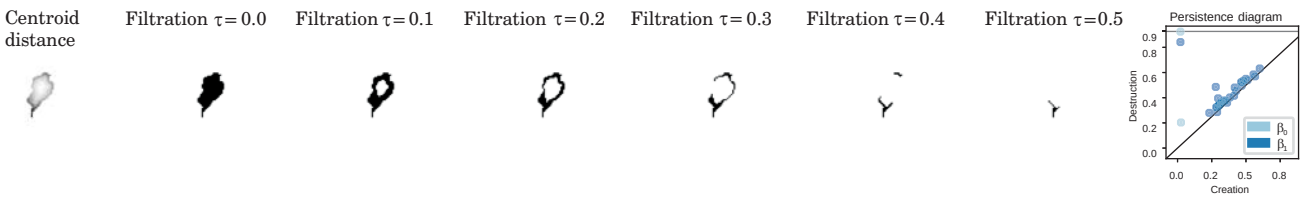

■ ***Fig. 2.*** An example of the filtration process

The choice of filtration in persistent homology determines the type of information that is captured about cycles, ranging from purely topological to a combination of topological and geometric information. Specific topological invariants exhibit robustness under affine transformations, whereas geometric invariants do not necessarily possess this property. As a result, the choice of filtration has significant implications for the persistence and importance of cycles, influencing which cycles are deemed significant and which are considered noise and less relevant [33]. To capture boundary information of shape we introduce filtration based on distance to the centroid of binary mask.

Lets V be a gray-scale volume, $V = [x_{dhw}]$ where x_{dhw} is the gray-scale value of the voxel (d, h, w), $d \in \{1, 2, \ldots, n_1\}$, $h \in \{1, 2, \ldots, n_2\}$, $w \in \{1, 2, \ldots, n_3\}$. First, we define a radial filtration function as l_2-norm distance between centroid of the binary mask and the reference point:

$$\varphi_r = \begin{cases} \left\| (d, h, w) - (d_0, h_0, w_0) \right\|_2, & x_{dhw} \geq x_0; \\ 0, & \text{otherwise}, \end{cases}$$

where (d, h, w) is the reference point for which the distance is calculated, x_0 is the gray-scale threshold, we take threshold value $x_0 = 0.5\max(V)$. We use centroid of the binary mask as the reference point (d_0, h_0, w_0) for radial filtration. The centroid is defined as a simple spatial average.

To capture information not only about topological features, but also about shape information the final filtration function defined as $\varphi = \varphi_r(1 - \varphi_{edt})$, where φ_{edt} is euclidean distance transform filtration which calculates the distance by replacing each foreground element on the mask with its shortest distance to the background.

In Figure 3 we visualize different filtration functions for the same nodule slice and their persistence diagrams. The first plot shows an slice of the nodule patch, the next two plots respectively show filtrations by centroid distance and euclidean distance for this slice, and three plots of persistence diagrams.

Topological constraints

Given a true likelihood function f and a predicted likelihood function f' and corresponding persistence diagrams D and D' we use Wasserstein distance to compare these diagrams. So, our topological loss can be defined as

$$L_T = \sum_{k=0}^{d} W_p(D_f^{(k)}, D_{f'}^{(k)}),$$

where $W_p(D_f^{(i)}, D_{f'}^{(i)})$ is a Wasserstein distance between persistence diagrams. This loss term

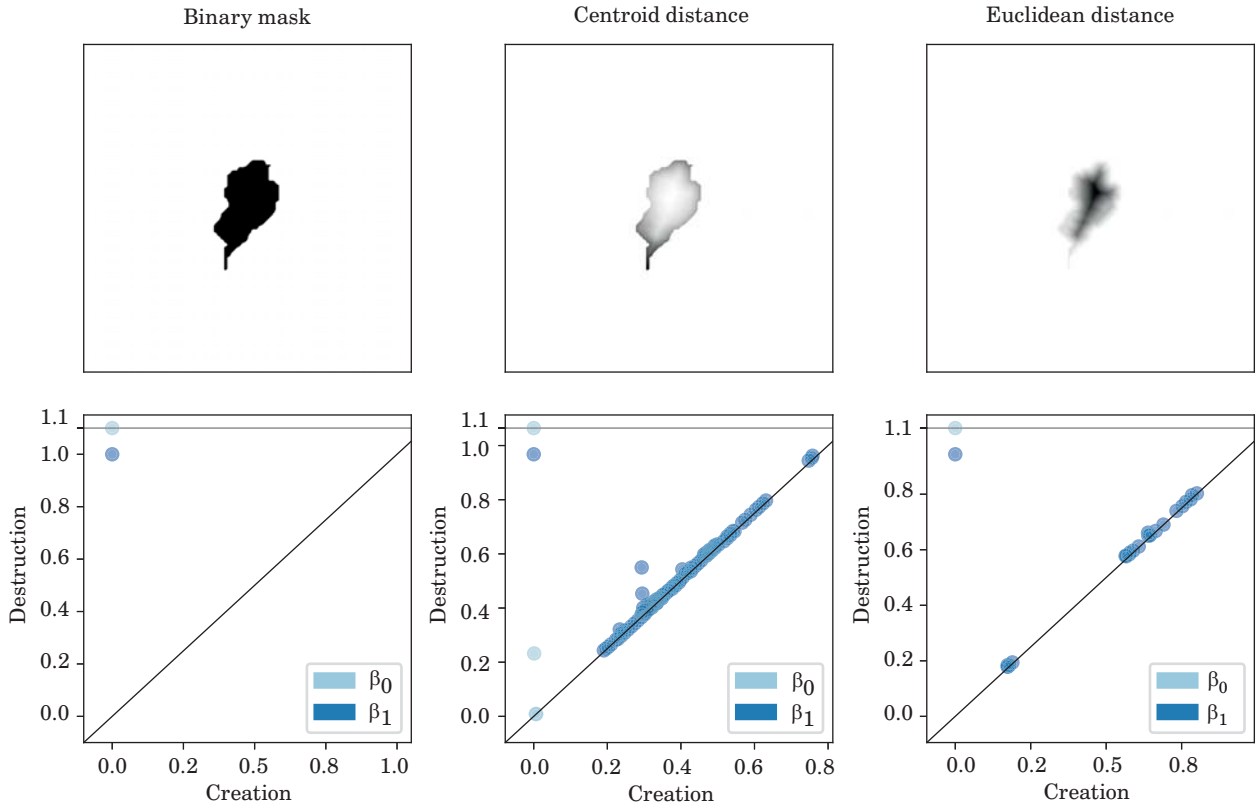

■ ***Fig. 3.*** Comparison of different filtrations and their persistence diagrams

encourages the model to reduce the distance between f and f' with respect to their topological shape and boundary information.

In the training pipeline with topological constraints during optimization of the L_T the Dice loss L_{Dice} landscape is flat in regions where there is no overlap between the prior and the ground truth due to, we regularize the shape and boundary reconstruction. The result is a limited and local modification of the prior that does not extend to the point of intersecting with the ground truth, and as a result the loss remains unchanged. To prevent the loss landscape from entering flat regions we propose a centroid loss that encourages the alignment of centroids between the predicted mask and the ground truth.

Proposed centroid loss can be defined as

$$L_C = \sqrt{\left\|(d_f, h_f, w_f) - (d_{f'}, h_{f'}, w_{f'})\right\|_2},$$

where (d_f, h_f, w_f) and $(d_{f'}, h_{f'}, w_{f'})$ are centroids of the prior and the ground truth respectively.

To jointly optimize the segmentation network the final loss can be defined as

$$L = L_{Dice} + \lambda_T L_T + \lambda_C L_C,$$

where λ_T and λ_C controls the impact of the corresponding loss terms.

Experiments

Datasets

The performance of our proposed training pipeline was evaluated using the publicly available LIDC-IDRI dataset [34], a comprehensive collection of CT scans from 1,010 patients, featuring annotated nodules that were identified and outlined by multiple radiologists from various medical institutions across the United States, employing a range of imaging protocols and scanner models from four different manufacturers.

We selected nodules that had a diameter in a range 5–50 mm, had minimum 1000 voxels in annotation, correct annotations and slice spacing in related scan and were identified by at least one radiologist. As a result, we had 393 nodule samples from LIDC-IDRI dataset, which divided into a training dataset of 282 samples, validation dataset of 32 samples and test dataset of 79 samples. We make sure that no sample is included in either the training, validation or test dataset.

Evaluation metrics

We use three main instance-level evaluation metrics to measure the instance segmentation performance of the comparison models: Jaccard index (JI), Dice score (DSC) and Hausdorff distance (HD) [35]. Jaccard index can be calculated as

$$JI = \frac{\left|Y_{true} \cap Y_{pred}\right|}{\left|Y_{true} \cup Y_{pred}\right|}.$$

It measures the ratio of the intersection and the union between the ground truth mask and predicted mask. Dice score focuses on the ratio of the intersection and the sum of the sets and penalizes differences less strictly because the denominator doesn't grow as fast as in the Jaccard index. Dice score can be defined as

$$DSC = \frac{2\left|Y_{true} \cap Y_{pred}\right|}{\left|Y_{true}\right| + \left|Y_{pred}\right|}.$$

Also we obtained additional performance metrics based on Minkowski functionals: volume error, surface area error, mean curvature error, which are calculated as the difference between the values of the corresponding n-th functional between the predicted mask and the ground truth:

$$M_n^{error} = \frac{\left|M_n^f - M_n^{f'}\right|}{M_n^f},$$

where M_n^f and $M_n^{f'}$ are corresponding Minkowski functional of the ground truth and the prior.

Implementation details

To extract the volume of interest for each nodule in our image processing workflow, we employ the pylidc package, a specialized library designed for the LIDC-IDRI dataset [36]. All patches are resampled to $0.75 \times 0.75 \times 0.75$ mm physical space and cropped to the resolution $96 \times 96 \times 96$ voxels using linear interpolation. Then we clamp intensity values (Hounsfield units) of volumes into a range [–1000, 1000] and rescale intensity values to a range [0, 1] with contrast stretching, as done in previous studies [37]. To implement processing pipeline for 3D data we use TorchIO library [38]. To calculate Minkowski functionals we use QuantImPy library [39].

The DeepLabV3 [40] architecture is employed as our target model, and in order to guarantee a fair comparison, we maintain a consistent implementation and hyperparameters setting throughout the entirety of our experiments, we employ "Weights and Biases" for tracking experiments [41]. The network are trained from imagenet weights for 200 epochs with a batch size of 28. We use the Adam optimizer with a dynamic learning rate (cosine annealing warm restarts [42]) from the start value 6×10^{-5} to the maximum value 1×10^{-4}. The op-

timizer has the first moment estimate 0.9 and the second moment estimate 0.999.

Also we optimize λ_T and λ_C parameters on an independent data set, as a result we used $\lambda_T = 0.02$ and $\lambda_C = 1.0$ for all experiments. These parameter values are chosen because the topological loss term is based on the Wasserstein distance between persistence diagrams and compares multi-scale topological features across the entire volume, which can yield relatively large numerical values. Larger λ_T parameter values can destabilize the model training process (topological features can be noisy at early training stages). Target shape for the interpolation step in topological descriptor was $18 \times 18 \times 18$ voxels because it's optimal in terms of performance and errors.

We augment the training data using standard image data augmentation techniques. This included randomly applying transformations such as reverse the order of elements in a volume along the axes, random rotating the input patch in a range [–25, 25] degrees and random affine transformation. To maintain consistency, we apply identical transformations to all slices within a nodule volume. Furthermore, we randomize the order of training examples in the each epoch. Our models and training pipeline are built using PyTorch and data processing pipeline is built with TorchIO and Torchvision libraries. The source code for the implementation of models and the training pipeline, data processing and dataset preparation is available at the link: https://github.com/dumaevrinat/ph_constraints.

Experiment results and discussion

To evaluate the benefits of our topological constraints, we perform the same experiment twice: in first run we use Dice loss only, and then added $\lambda_T L_T$ and $\lambda_C L_C$ loss terms. As shown in Table, our training pipeline with topological constraints outperforms the baseline across all three main metrics. We also provide error comparison based on Minkowski functionals. The volume error, surface area error, and mean curvature error are all also slightly lower for the approach with topological constraints. We perform a paired Wilcoxon signed-rank test between the two error distributions, the obtained p-values are also presented in the Table. We show a detailed comparison of $1 - DSC$ (fig. 4, *a*) and $1 - JI$ (fig. 4, *b*) evaluation metrics on different groups of nodules divided into quartiles by volume and surface area.

The results of comparing two approaches to model training, with and without topological constraints, indicate that incorporating topological constraints leads to improved lung nodule segmentation performance.

The effectiveness of the proposed segmentation method with topological constraints is illustrated in the Fig. 5. The segmentation results (one slice from the whole segmentation volume) for four example nodules from the test dataset are compared against the baseline approach, with invalid regions shown as red rectangles. The baseline method exhibits inconsistencies such as fragmented boundaries and isolated false-positive regions. In contrast, method based on persistent homology-based constraints produces more closely segmentations to the ground truth. This improvement is especially noticeable in the absence of topological errors such as holes or unconnected components.

■ Lung nodule segmentation performance of different training pipelines

Evaluation metric	Without topological constraints	With topological constraints	p-value
1 – DSC	0.33 ± 0.20	0.29 ± 0.16	0.0103
1 – JI	0.46 ± 0.19	0.43 ± 0.17	0.0056
HD	7.74 ± 5.05	6.09 ± 5.70	0.0094
M_0 (volume error)	0.29 ± 0.32	0.30 ± 0.29	0.0465
M_1 (surface area error)	0.22 ± 0.25	0.19 ± 0.23	0.0158
M_2 (mean curvature error)	0.26 ± 0.21	0.21 ± 0.22	0.0002

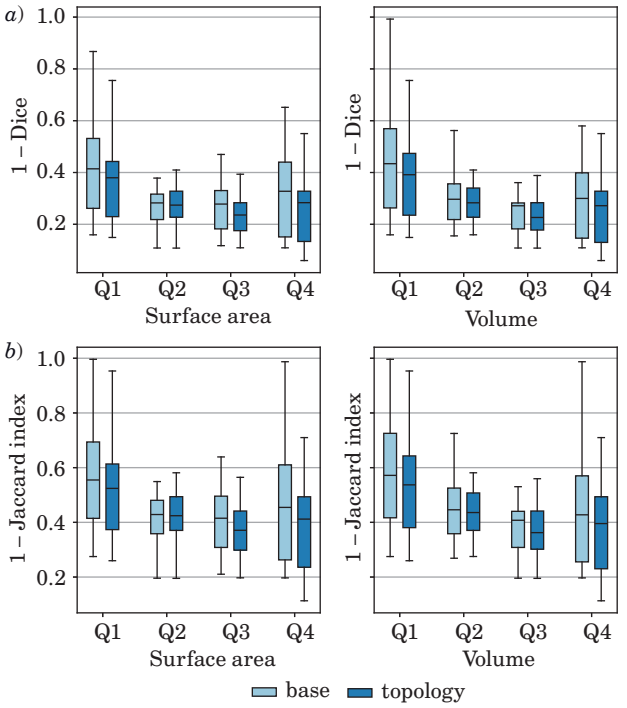

■ ***Fig. 4.*** Comparison of Dice (*a*) and Jaccard (*b*) loss metric for base and topological pipelines for samples divided into quartiles by surface area and volume

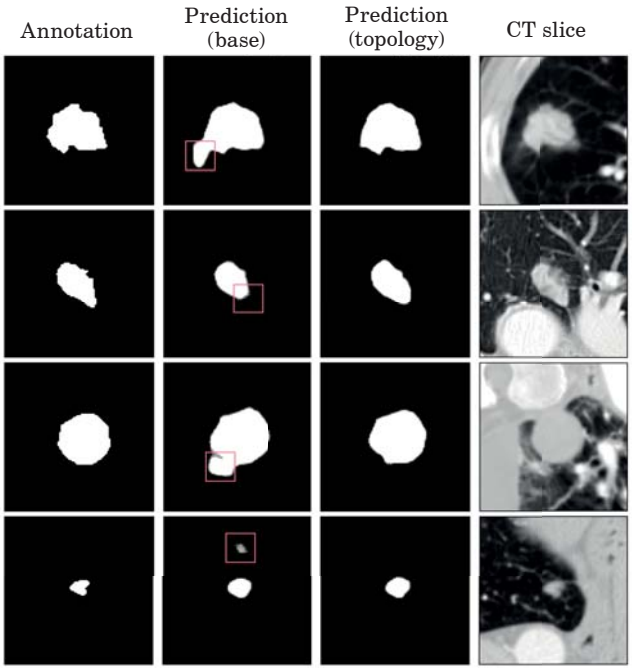

■ ***Fig. 5.*** Comparison of lung nodule segmentation results

The proposed method integrates persistent homology-based topological constraints into 3D medical image segmentation, demonstrating improved performance over traditional pixel-wise loss functions. By leveraging TDA, our approach ensures that predicted segmentations adhere to expected morphological properties and boundary consistency. Below, we discuss our results, compare our method with existing approaches, and outline its limitations and potential applications.

Most deep learning-based segmentation methods focus on improving accuracy through architectural modifications or post-processing. These approaches often ignore topological correctness. Recent works have explored topology-aware losses, but many of them rely on simplifying assumptions such as fixed Betti numbers [25], which lack the multi-scale flexibility of persistent homology. In contrast, our method captures topological and shape representation features across varying scales through persistence diagrams.

Despite the above advantages, our method has several limitations. The topological loss assumes high-quality ground truth annotations. In practice, variability in medical annotations from multiple experts may require robustness to noisy labels. Calculating persistent homology for high-resolution 3D volumes is computationally intensive and requires CPU resources. Although downsampling mitigates this to some extent, future work may focus on exploring this limitation.

Although the effectiveness of the method has been confirmed in pulmonary lung nodules, further studies are needed for other types of lesions.

Conclusion

In this paper, we proposed persistent homology-based topological constraints and their integration into medical image segmentation represents a significant advancement in the field, particularly for applications such as lung nodule detection. By employing a new filtration function based on centroid distance, the proposed method effectively refines shape and boundary representation and improves the accuracy of segmentation.

Empirical results (see Table) for lung nodule segmentation using 3D computed tomography images validate the effectiveness of our framework. The results indicate that this approach not only improves pixel-level accuracy but also preserves essential morphological properties, which are critical for downstream applications such as volume estimation and clinical decision-making.

Future studies and improvements in topology-aware methods may further increase the accuracy and usefulness of automated segmentation tools, ultimately leading to improved patient outcomes in clinical settings. The current evolution of TDA within machine learning has great potential to improve understanding and interpretation of complex medical images.

Financial support

The research is partially funded by the Ministry of Science and Higher Education of the Russian Federation as part of state assignments, topic FSEG-2024-0027.

References

1. Wang S., Zhou M., Liu Z., Liu Z., Gu D., Zang Y., Dong D., Gevaert O., Tian J. Central focused convolutional neural networks: Developing a data-driven model for lung nodule segmentation. *Medical Image Analysis*, 2017, vol. 40, pp. 172–183. doi:10.1016/j.media.2017.06.014
2. de Margerie-Mellon C., Chassagnon G. Artificial intelligence: A critical review of applications for lung nodule and lung cancer. *Diagnostic and Interventional Imaging*, 2023, vol. 104, no. 1, pp. 11–17. doi:10.1016/j.diii.2022.11.001
3. Callister M., Baldwin D., Akram A., Barnard S., Cane P., Draffan J., Franks K., Gleeson F., Graham R., Malhotra P. British thoracic society guidelines for the

investigation and management of pulmonary nodules: Accredited by nice. *Thorax*, 2015, vol. 70, no. Suppl 2, pp. ii1–ii54. doi:10.1136/thoraxjnl-2015-207168
4. Dong T., Wei L., Nie S. Research progress of lung nodule segmentation based on CT images. *Journal of Image and Graphics*, 2021. Available at: https://api.semanticscholar.org/CorpusID:273256366 (accessed 15 December 2024).
5. Agnes S. A., Anitha J. Efficient multiscale fully convolutional unet model for segmentation of 3D lung nodule from CT image. *Journal of Medical Imaging*, 2022, vol. 9, no. 5, pp. 052402–052402. doi:10.1117/1.JMI.9.5.052402
6. Chartrand G., Cheng P. M., Vorontsov E., Drozdzal M., Turcotte S., Pal C. J., Kadoury S., Tang A. Deep learning: A primer for radiologists. *Radiographics*, 2017, vol. 37, no. 7, pp. 2113–2131. doi:10.1148/rg.2017170077
7. Ronneberger O., Fischer P., Brox T. U-Net: Convolutional networks for biomedical image segmentation. *18th International Conference Medical Image Computing and Computer-Assisted Intervention — MICCAI*, 2015, pp. 234–241. doi:10.1007/978-3-319-24574-4_28
8. Duan J., Bello G., Schlemper J., Bai W., Dawes T. J., Biffi C., de Marvao A., Doumoud G., O'Regan D. P., Rueckert D. Automatic 3D bi-ventricular segmentation of cardiac images by a shape-refined multi-task deep learning approach. *IEEE Transactions on Medical Imaging*, 2019, vol. 38, no. 9, pp. 2151–2164. doi:10.1109/TMI.2019.2905196
9. Hensel F., Moor M., Rieck B. A survey of topological machine learning methods. *Frontiers in Artificial Intelligence*, 2021, vol. 4, Article 681108.
10. Xie H., Yang D., Sun N., Chen Z., Zhang Y. Automated pulmonary nodule detection in CT images using deep convolutional neural networks. *Pattern Recognition*, 2019, vol. 85, pp. 109–119. doi:10.1016/j.patcog.2018.08.006
11. Pezzano G., Ripoll V. R., Radeva P. Cole-CNN: Context-learning convolutional neural network with adaptive loss function for lung nodule segmentation. *Computer Methods and Programs in Biomedicine*, 2021, vol. 198, Article 105792. doi:10.1016/j.cmpb.2020.105792
12. Wu D., Lu L., Bi J., Shinagawa Y., Boyer K., Krishnan A., Salganicoff M. Stratified learning of local anatomical context for lung nodules in CT images. *2010 IEEE Computer Society Conference on Computer Vision and Pattern Recognition*. IEEE, 2010, pp. 2791–2798. doi:10.1109/CVPR.2010.5540027
13. Cao H., Liu H., Song E., Hung C.-C., Ma G., Xu X., Jin R., Lu J. Dual-branch residual network for lung nodule segmentation. *Applied Soft Computing*, 2020, vol. 86, Article 105934. doi:10.1016/j.asoc.2019.105934
14. Zhou Z., Gou F., Tan Y., Wu J. A cascaded multi-stage framework for automatic detection and segmentation of pulmonary nodules in developing countries. *IEEE Journal of Biomedical and Health Informatics*, 2022, vol. 26, no. 11, pp. 5619–5630. doi:10.1109/JBHI.2022.3196842
15. Yang H., Wang Q., Zhang Y., An Z., Liu C., Zhang X., Zhou S. K. Lung nodule segmentation and uncertain region prediction with an uncertainty-aware attention mechanism. *IEEE Transactions on Medical Imaging*, 2023, vol. 43, no. 4, pp. 1284–1295. doi:10.1109/TMI.2023.3348698
16. Dumaev R. I., Molodyakov S. A., Utkin L. V. A model for explainable malignancy assessment of pulmonary nodules on CT images. *Artificial Intelligence and Decision Making*, 2024, no. 4, pp. 123–134.
17. Byrne N., Clough J. R., Valverde I., Montana G., King A. P. A persistent homology-based topological loss for CNN-based multiclass segmentation of CMR. *IEEE Transactions on Medical Imaging*, 2022, vol. 42, no. 1, pp. 3–14. doi:10.1109/TMI.2022.3207234
18. Hu X., Li F., Samaras D., Chen C. Topology-preserving deep image segmentation. *Advances in Neural Information Processing Systems*, 2019, vol. 32, pp. 5657–5668.
19. Mosinska A., Marquez-Neila P., Kozin'ski M., Fua P. Beyond the pixel-wise loss for topology-aware delineation. *Proceedings of the IEEE Conference on Computer Vision and Pattern Recognition*, 2018, pp. 3136–3145. doi:10.1109/CVPR.2018.00331
20. Demir A., Massaad E., Kiziltan B. Topology-aware focal loss for 3D image segmentation. *Proceedings of the IEEE/CVF Conference on Computer Vision and Pattern Recognition*, 2023, pp. 580–589. doi:10.1109/CVPR52729.2023.00061
21. de Dumast P., Kebiri H., Dunet V., Koob M., Cuadra M. B. Multi-dimensional topological loss for cortical plate segmentation in fetal brain MRI. *arXiv preprint* arXiv:2208.07566, 2022.
22. Skaf Y., Laubenbacher R. Topological data analysis in biomedicine: A review. *Journal of Biomedical Informatics*, 2022, vol. 130, Article 104082. doi:10.1016/j.jbi.2022.104082
23. Singh Y., Farrelly C. M., Hathaway Q. A., Leiner T., Jagtap J., Carlsson G. E., Erickson B. J. Topological data analysis in medical imaging: Current state of the art. *Insights into Imaging*, 2023, vol. 14, no. 1, p. 58. doi:10.1186/s13244-023-01410-z
24. Wen B., Zhang H., Bartsch D.-U. G., Freeman W. R., Nguyen T. Q., An C. Topology-preserving image segmentation with spatial-aware persistent feature matching. *arXiv preprint* arXiv:2412.02076, 2024.
25. Clough J. R., Byrne N., Oksuz I., Zimmer V. A., Schnabel J. A., King A. P. A topological loss function for deep-learning based image segmentation using persistent homology. *IEEE Transactions on Pattern Analysis and Machine Intelligence*, 2020, vol. 44, no. 12, pp. 8766–8778. doi:10.1109/TPAMI.2020.2994504
26. Sun S., Wang Y., Yang J., Feng Y., Tang L., Liu S., Ning H. Topology-sensitive weighting model for myocardial segmentation. *Computers in Biology and Med-*

icine, 2023, vol. 165, Article 107286. doi:10.1016/j.compbiomed.2023.107286

27. Qaiser T., Tsang Y.-W., Taniyama D., Sakamoto N., Nakane K., Epstein D., Rajpoot N. Fast and accurate tumor segmentation of histology images using persistent homology and deep convolutional features. *Medical Image Analysis*, 2019, vol. 55, pp. 1–14. doi:10.1016/j.media.2019.04.005

28. Qaiser T., Sirinukunwattana K., Nakane K., Tsang Y.-W., Epstein D., Rajpoot N. Persistent homology for fast tumor segmentation in whole slide histology images. *Procedia Computer Science*, 2016, vol. 90, pp. 119–124. doi:10.1016/j.procs.2016.07.040

29. François A., Tinarrage R. Train-free segmentation in MRI with cubical persistent homology. *arXiv preprint* arXiv:2401.01160, 2024.

30. Rieck B., Yates T., Bock C., Borgwardt K., Wolf G., Turk-Browne N., Krishnaswamy S. Uncovering the topology of time-varying fMRI data using cubical persistence. *Advances in Neural Information Processing Systems*, 2020, vol. 33, pp. 6900–6912.

31. Stucki N., Paetzold J. C., Shit S., Menze B., Bauer U. Topologically faithful image segmentation via induced matching of persistence barcodes. *International Conference on Machine Learning*, *PMLR*, 2023, pp. 32698–32727.

32. Stucki N., Bürgin V., Paetzold J. C., Bauer U. Efficient Betti matching enables topology-aware 3D segmentation via persistent homology. *arXiv preprint* arXiv:2407.04683, 2024.

33. Turkes R., Nys J., Verdonck T., Latre S. Noise robustness of persistent homology on greyscale images, across filtrations and signatures. *PLOS ONE*, 2021, vol. 16, no. 9, Article e0257215. doi:10.1371/journal.pone.0257215

34. Armato S. G. III, McLennan G., Bidaut L., McNitt-Gray M. F., Meyer C. R., Reeves A. P., Zhao B., Aberle D. R., Henschke C. I., Hoffman E. A., Kazerooni E. A., MacMahon H., Van Beek E. J. R., Yankelevitz D., Biancardi A. M., Bland P. H., Brown M. S., Engelmann R. M., Laderach G. E., Clarke L. P. The lung image database consortium (LIDC) and image database resource initiative (IDRI): A completed reference database of lung nodules on CT scans. *Medical Physics*, 2011, vol. 38, no. 2, pp. 915–931. doi:10.1118/1.3528204

35. Karimi D., Salcudean S. E. Reducing the hausdorff distance in medical image segmentation with convolutional neural networks. *IEEE Transactions on Medical Imaging*, 2019, vol. 38, no. 2, pp. 499–513.

36. Hancock M. C., Magnan J. F. Lung nodule malignancy classification using only radiologist-quantified image features as inputs to statistical learning algorithms: Probing the lung image database consortium dataset with two statistical learning methods. *Journal of Medical Imaging*, 2016, vol. 3, no. 4, Article 044504. doi:10.1117/1.JMI.3.4.044504

37. Isensee F., Petersen J., Klein A., Zimmerer D., Jaeger P. F., Kohl S., Wasserthal J., Koehler G., Norajitra T., Wirkert S. nnU-Net: Self-adapting framework for U-Net-based medical image segmentation. *arXiv preprint* arXiv:1809.10486, 2018.

38. Pérez-García F., Sparks R., Ourselin S. TorchIO: a Python library for efficient loading, preprocessing, augmentation and patch-based sampling of medical images in deep learning. *Computer Methods and Programs in Biomedicine*, 2021, Article 106236. Available at: https://www.sciencedirect.com/science/article/pii/S0169260721003102 (accessed 15 December 2024).

39. Boelens A. M., Tchelepi H. A. Quantimpy: Minkowski functionals and functions with Python. *SoftwareX*, 2021, vol. 16, Article 100823. doi:10.1016/j.softx.2021.100823

40. Chen L.-C. Rethinking atrous convolution for semantic image segmentation. *arXiv preprint* arXiv:1706.05587, 2017.

41. Biewald L. *Experiment tracking with weights and biases*. 2020. Software available from wandb.com. Available at: https://www.wandb.com/ (accessed 15 December 2024).

42. Loshchilov I., Hutter F. SGDR: Stochastic gradient descent with warm restarts. *arXiv preprint* arXiv:1608.03983, 2016.

УДК 004.852
doi:10.31799/1684-8853-2025-4-2-12
EDN: ZRIITM

Сегментация медицинских 3D-изображений с использованием персистентных гомологий

Р. И. Думаев[a], аспирант, orcid.org/0009-0002-3674-4952
С. А. Молодяков[a], доктор техн. наук, профессор, orcid.org/0000-0003-2191-9449, samolodyakov@mail.ru
Л. В. Уткин[a], доктор техн. наук, профессор, orcid.org/0000-0002-5637-1420
[a]Санкт-Петербургский политехнический университет Петра Великого, Политехническая ул., 29, Санкт-Петербург, 195251, РФ

Введение: традиционные подходы к обучению моделей сегментации часто опираются на функции потерь по вокселям, что недостаточно для многих задач сегментации, и не учитывают топологическую корректность сегментации. Следовательно, маски, полученные с помощью таких моделей, могут быть пространственно несогласованны, что приводит к появлению нереалистичных харак-

теристик, таких как ложные связанные компоненты или дыры. **Цель:** разработать метод обучения моделей для повышения качества сегментации медицинских 3D-изображений за счет использования персистентных гомологий и сравнения диаграмм персистентности в процессе обучения. **Результаты:** предложен метод обучения моделей сегментации 3D-изображений, включающий ограничения на основе персистентных гомологий и функцию потерь, которая применяется для регуляризации процесса восстановления формы и краев маски. Представлена функция фильтрации, основанная на расстоянии до центроида бинарной маски, для уточнения формы и границы предсказанной маски. Анализ результатов, полученных в ходе экспериментов на данных компьютерной томографии легких для задачи сегментации и выделения целевых структур, показал эффективность предложенного метода. Он не только повышает точность на уровне вокселей, но и сохраняет существенные морфологические свойства, что крайне важно для последующих задач, таких как оценка объема узелков и принятие клинических решений. **Практическая значимость:** использование представленного метода позволило повысить качество сегментации легочных узелков по 3D-изображениям компьютерной томографии.

Ключевые слова — сегментация медицинских изображений, предсказание формы, топологический анализ данных, персистентная гомология, сегментация узелков в легких.

Для цитирования: Dumaev R. I., Molodyakov S. A., Utkin L. V. 3D medical image segmentation with persistent homology-based constraints. *Информационно-управляющие системы*, 2025, № 4, с. 2–12. doi:10.31799/1684-8853-2025-4-2-12, EDN: ZRIITM
For citation: Dumaev R. I., Molodyakov S. A., Utkin L. V. 3D medical image segmentation with persistent homology-based constraints. *Informatsionno-upravliaiushchie sistemy* [Information and Control Systems], 2025, no. 4, pp. 2–12. doi:10.31799/1684-8853-2025-4-2-12, EDN: ZRIITM

УВАЖАЕМЫЕ АВТОРЫ!

Научные базы данных, включая Scopus и Web of Science, обрабатывают данные автоматически. С одной стороны, это ускоряет процесс обработки данных, с другой — различия в транслитерации ФИО, неточные данные о месте работы, области научного знания и т. д. приводят к тому, что в базах оказывается несколько авторских страниц для одного и того же человека. В результате для всех по отдельности считаются индексы цитирования, что снижает рейтинг ученого.

Для идентификации авторов в сетях Thomson Reuters проводит регистрацию с присвоением уникального индекса (ID) для каждого из авторов научных публикаций.

Процедура получения ID бесплатна и очень проста, есть возможность провести регистрацию на 12 языках, включая русский (чтобы выбрать язык, кликните на зеленое поле вверху справа на стартовой странице): https://orcid.org